BJRS
BRAZILIAN JOURNAL OF RADIATION SCIENCES

doi.org/10.15392/2319-0612.2024.2469
2024, 12(3A) | 01-21 | e2469
Submitted: 2024-03-25
Accepted: 2024-09-11

Development of a Methodology for Measuring the Output Factor for Electron Blocks

Fontana[a*], J. M.; Santos[a], M. R.

[a] National Cancer Institute - INCA, Postal code: 20230130, Rio de Janeiro, RJ, Brasil.

*Correspondence: jumarfon@gmail.com

Abstract: In light of the routine verification of output factor for electron blocks manufactured for patients and outside the standard square field measurements, this study proposes a methodology for measuring the output factor using EPID, validated by water measurements with a diode, and employing Python programming to analyze the pre-processed detector images. The study used square and rectangular blocks to validate the code and evaluate the limitations of the EPID, finding an agreement of up to ±3.0% for fields larger than 6.0 cm² and ±5.0% for fields between 3.0 cm² and 5.0 cm². The final evaluation aimed to compare square field measurements with asymmetric rectangular fields, and the results showed deviations of less than ±1.0%, thus indicating the feasibility of using EPID for this methodology.

Keywords: Radiotherapy; electrons beams; output factor; EPID; Python.

BJRS
BRAZILIAN JOURNAL OF RADIATION SCIENCES

doi.org/10.15392/2319-0612.2024.2469
2024, 12(3A) | 01-21 | e2469
Submitted: 2024-03-25
Accepted: 2024-09-11

Desenvolvimento de metodologia para medição do fator output para blocos de elétrons

Resumo: Diante do cenário da rotina de verificação de fator output para blocos de elétrons manufaturados para pacientes e fora do padrão das medidas quadradas, o presente trabalho propõe uma metodologia de medida do fator output no EPID, validando com medida em água usando diodo e utilizando programação em Python para analisar as imagens pré-processadas do detector. O trabalho utilizou blocos quadrados e retangulares para validar o código e avaliar as limitações do EPID e encontrou concordância de até ±3,0% para campos maiores que 6,0 cm² e ±5,0% para campos entre 3,0 cm² e 5,0 cm². A última avaliação realizada teve o intuito de confrontar as medidas do campo quadrado com campos assimétricos retangulares e os resultados obtiveram desvios menores que ±1,0%, indicando assim a viabilidade do EPID para tal metodologia.

Palavras-chave: Radioterapia; feixes de elétrons; fator output; EPID; Python.

SBPR

1. INTRODUCTION

For the period from 2023 to 2025, oncological projections indicate that in Brazil there will be approximately 704 thousand new cases of cancer, with 483 thousand, excluding non-melanoma skin cancer. Non-melanoma skin cancer is projected to be the most prevalent type, with 220 thousand new cases (31.3%) [1].

One of the treatment modalities for most non-melanoma skin cancers (the most frequent being basal cell carcinoma and squamous cell carcinoma) and melanoma, when superficial, is electron beam radiotherapy. In practice, currently, electron beams account for about 10% to 15% of the total treatments performed. The availability of clinical electron beams in linear accelerators allows for the provision of various teletherapy treatment modalities. Equipment with photon beams of 6 and 10 MV, along with six electron energies ranging from 4 to 16 MeV, are considered ideal for installation in medium and large centers nationwide. This diversity of energies facilitates therapeutic adaptation, allowing for precise adjustments for geometry, dimension, depth, coverage, and dose distribution in the disease. Remarkably, electron beams, especially those of lower energy, are rapidly absorbed by tissues, resulting in a rapid decrease in depth, minimizing exposure to deeper tissues, beyond the area of interest [2].

In addition to superficial tumors, electron beam treatment is effective for various hyperproliferative disorders and benign conditions, such as keloids, mycosis, peritendinitis, calcaneal spur, plantar fasciitis, and osteoarthritis. This enables the application of different therapeutic protocols and dose fractionation schemes, which can be included as a primary or complementary therapeutic approach, resulting in high rates of local control and analgesia [3].

Radiotherapy has been revealed as the most effective method in preventing keloid recurrence [4]. Furthermore, there is a genetic influence on this phenomenon, being more

prevalent in Asians, Hispanics, and Africans compared to Caucasians [5,6,7,8,9]. Brazil ranks second globally in plastic surgeries, with 2.5 million procedures [10]. Keloids can occur in 5.0% to 15.0% of surgical wounds, and in inevitable cases, minimizing skin tension is crucial. Immediate keloid treatment reduces the risk of new lesions [11].

The crucial point for calculating electron beam treatments lies in defining the output factors for irregular fields or small apertures, requiring greater care in measurements and the choice of detector to obtain these factors. Commonly used detectors are ionization chambers or diodes. Both have advantages and disadvantages regarding accuracy, reproducibility, and geometric limitations, and it is up to the medical physicist to know these factors for appropriate selection for such measurements. In this work, the use of diodes was chosen due to their high spatial resolution, necessary for evaluating fields with smaller apertures.

In the routine of superficial treatments with electron beams, during simulation, irregular field apertures can be defined, different from pre-commissioned ones, requiring an output factor measurement to reduce uncertainty in planning, which is related to the correction due to scattered radiation throughout the collimation system and phantom [12].

The output factor is described in the literature as the product of the cutout factor and the applicator factor, where the cutout factor is obtained by the ratio of readings using the frame with the cutout of the block and the open frame of the applicator used, and the applicator factor is defined by the ratio of readings with the open frame of the applicator used and with the open frame of the reference applicator. Thus, the output factor can be simplified, as shown in figure 1, which is the definition of the output factor adopted in this work.

Figure 1: Demonstration of the output factor equation used in the study.

$$\text{Output Factor} = \text{Cutout Factor} \times \text{Applicator Factor}$$

$$\text{Output Factor} = \frac{\text{Block Frame Reading}}{\text{Open Frame Reading}} \times \frac{\text{Open Frame Reading}}{\text{Reference Frame Reading}}$$

$$\text{Output Factor} = \frac{\text{Block Frame Reading}}{\text{Reference Frame Reading}}$$

Due to the possibility of defining irregular fields, the need for a quick and simplified verification for pre-treatment quality control was identified, aiming to determine the output factor more accurately in this scenario, reducing uncertainties compared to common practices of estimating factors, that as seen in a systematic review of the literature, there are several methods for assuming this Variable [12,13,18,19,20,21].

Given that the measurement of collimation blocks is fundamental for electron beams and the output factor is used to correct this emission, the literature indicates variations between 2.0% and 40.0% of dose. The impact varies with the aperture radius, decreasing as this radius increases [13].

Considering the significant use of the EPID (Electronic Portal Imaging Device), which is an array of photodiode detectors immersed in a layer of amorphous silicon (aSi), with the detection unit composed of three layers - the outermost layer of 1 mm of copper, used to remove low-energy photons and electrons produced in the patient; the second layer of scintillator material (Gd2O2S:Tb), of micrometer thickness, and the photodiodes of the third layer, which are deposited on a thin film transistor in a matrix of 512 x 384 elements in an area of 40 x 30 cm². The electronic signal obtained in each element is read separately, and the processing of all signals together gives rise to the raw image of the EPID [14].

This device is enabled to measure matrices of accumulated dose, comparing planned and irradiated doses, subsequently interpreted by software that uses a methodology to

quantify these dose distributions [14], and which has good sensitivity, ease of use, high spatial and temporal resolution, large active detection area, real-time acquisition, and rapid data processing [15], widely used as a detector for quality control in photon beams, there was a motivation for the development of a previous work in the institution so that the EPID could be used to perform measurements with electron beams [16,17].

In the previous work cited [17], which utilized the same equipment as this study and evaluated some dosimetric parameters for implementing quality control for electron beams using the EPID, such as linearity, dose rate dependence, short-term reproducibility, beam constancy on the central axis, and symmetry and flatness constancy. The results were highly satisfactory and consistent, demonstrating excellent short-term reproducibility (maximum of 0.02%), with maximum variations of 1.56% in beam constancy on the central axis relative to the reference, variation less than 0.40% for symmetry and flatness constancy, and no more than 0.34% variation in dose rate dependence.

Having done so, the present study suggests an application of using the EPID to validate the intended methodology for obtaining the output factor for calculating monitor units (MU) for electron beam plans.

2. MATERIALS AND METHODS

In a previous study carried out at the institution entitled "Implementation of Test for Electron Beam Quality Control using Varian EPID" (RIBEIRO; Rosane Moreira, 2023) it was a quality control study of electron beams on the EPID was performed, and a calibration file type *.xml was created, adapted for evaluating linearity, dose rate dependence, short-term reproducibility, beam constancy on the central axis, and symmetry and flatness constancy, saved in DICOM format and analyzed with a locally developed

program written in Python, which was validated for such measurements, whose results were satisfactory according to the literature [16,17].

The present study was divided into 3 stages (described below in items A, B, and C) of measurement on the Clinac CX Linear Accelerator (Varian Medical System, Las Vegas - USA) to demonstrate the methodology for measuring the output factor of electron blocks, always maintaining the Gantry, Collimator, and Table at 0° and performed with all available beam energies of the equipment (6 MeV, 9 MeV, 12 MeV, 15 MeV, and 18 MeV) and for the applicators of 6.0 cm^2, 10.0 cm^2, 15.0 cm^2, and 20.0 cm^2. Measurements for each field reading were made with 50.0 MU and a dose rate of 400.0 MU/min for both detectors used, diode and EPID.

For experimental validation, a diode (PTW Freiburg, model TN 60022) was used for relative measurements to determine the output factors, using the reference applicator (10.0 cm^2) at the reference depths for each energy, at a source-to-surface distance of 100.0 cm.

Regarding measurements on the EPID (Model aS1000 - ExactArm), the detector position was fixed at 105.0 cm from the focal point. Raw images (pre-processed) were extracted, considering only pixel-by-pixel counts. Thus, the device was calibrated to determine beam fluence, establishing a relationship between the values of the central pixel region of the EPID for the collimated field and for the reference field. The recorded EPID images were saved in DICOM format and manipulated using the Python language (v. 3.10 on the Google Collaboratory platform), associated with the Pydicom library (v. 2.4.4).

The code developed uses the raw image produced in the 4D Console, with dark field and flood field corrections. First, the DICOM image is converted into an array of the same resolution, and the algorithm is designed to locate the central region of the field apertures in the in-plane and cross-plane axes. The maximum profiles in both axes are extracted, and the average count value of the central 2 cubic millimeters is calculated. The same process is performed on the reference square field image, and the ratio between the two values

represents the calculated output factor. Thus, the value obtained by the code follows the same methodology as the commissioning performed at the institution.

The resulting data were analyzed using Excel program (Microsoft Windows) to quantify and tabulate the output factors found with the diode and EPID, as well as calculating the deviations between them. Deviations between experimental and calculated values in Python were calculated using the experimental values as a reference, and tolerances were set at ±3.0% as ideal and up to ±5.0% as acceptable [18,19].

Figure 2 illustrates the setup used for conducting the experimental measurements performed on the diode and EPID.

Figure 2: Illustration of the experimental setup used with diode and EPID.

A) Measurements with open square fields

The first stage of measurements in the study involves open symmetric square fields, with various field sizes, some already provided by the manufacturer and others constructed at the Institution using low melting point alloy - cerrobend, from the planning system in the workshop sector of INCA, with their dimensions presented in table 1.

Table 1: Sizes of corresponding blocks and applicators used.

Block Size (cm²)	Square Equivalent Field (SEF) (cm²)	Applicator (cm²)
3.0 x 3.0	3.0	6.0 x 6.0
4.0 x 4.0	4.0	6.0 x 6.0
5.0 x 5.0	5.0	6.0 x 6.0
6.0 x 6.0	6.0	6.0 x 6.0
8.0 x 8.0	8.0	10.0 x 10.0
10.0 x 10.0	10.0	10.0 x 10.0
12.0 x 12.0	12.0	15.0 x 15.0
15.0 x 15.0	15.0	15.0 x 15.0
17.0 x 17.0	17.0	20.0 x 20.0
20.0 x 20.0	20.0	20.0 x 20.0

Thus, each field was measured with the diode positioned at the central axis, in water and at the reference depth of each beam (as per table 2), with 3 measurements taken for each block, extracting the average of the readings normalized by the open 10.0 x 10.0 cm² frame, obtaining the output factor for each field. The same measurements were repeated on the EPID.

Table 2: Reference depths for each energy used.

Beam Energy (MeV)	Reference Depth (cm)
6.0	1.4
9.0	2.1
12.0	2.9
15.0	3.8
18.0	4.5

B) Measurements with open rectangular fields

The second stage involved measuring, both with the diode and the EPID, symmetric rectangular fields with the respective equivalent square fields (ESF) of the open fields from stage 1 (table 3), extracted using the Clarkson Method, along the central axis and SSD = 100.0 cm, fabricated in the Radiotherapy service of INCA.

Table 3: Dimensions of equivalent square fields.

Block Size (X x Y cm²)	SEF (cm²)	Applicator (cm²)
5.0 x 7.5	6.0	10.0 x 10.0
7.5 x 8.5	8.0	10.0 x 10.0
7.0 x 19.0	10.0	20.0 x 20.0
9.5 x 17.0	12.0	20.0 x 20.0
13.0 x 18.0	15.0	20.0 x 20.0

C) Measurements with asymmetric and half-blocked fields

The third stage of the study involved constructing and measuring half-blocked, asymmetric blocks, and off-center fields. These blocks will be analyzed by comparing only the output factor with EPID to analyze the influence and behavior of collimation on the central axis. For this purpose, the blocks listed in table 4 were manufactured.

Table 4: Size of half-blocked and asymmetric blocks.

Block Dimension (cm)	Block Size (cm²)	SEF (cm²)	Applicator (cm²)
x1 = 0.0; x2 = 4.0; y1 = 5.5; y2 = 5.5	4.0 x 11.0	6.0	15.0 x 15.0
x1 = 0.0; x2 = 6.0; y1 = 6.0; y2 = 6.0	6.0 x 12.0	8.0	15.0 x 15.0
x1 = 0.0; x2 = 7.0; y1 = 9.0; y2 = 9.0	7.0 x 18.0	10.0	20.0 x 20.0
x1 = 0.0; x2 = 9.0; y1 = 8.5; y2 = 8.5	9.0 x 17.0	12.0	20.0 x 20.0

The measurements were carried out with the EPID, following the same setup procedure mentioned earlier, for all energies. Each block was measured in the four possible positions of fitting the block into the applicator, as shown in figure 3, aiming to evaluate the output factor off the central axis, considering that there was no correction for beam symmetry and flatness, as evaluated in a previous study [17].

Figure 3: Example of the four acquired positions of the 7.0 cm x 18.0 cm block, referred to in the study as "below," "above," "right," and "left," respectively.

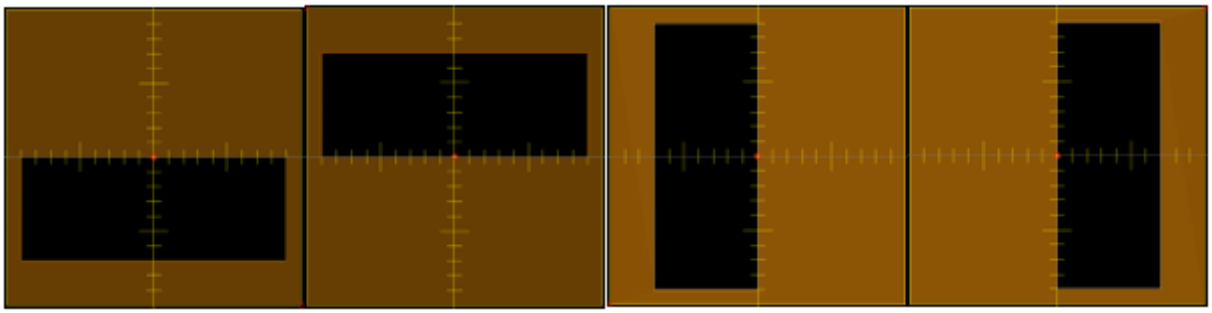

3. RESULTS AND DISCUSSIONS

A) Measurements with open square Fields

Table 5 encompasses the output factors and their respective percentage diferences between EPID and diode measurements of the open fields.

Table 5: Output factors and percentage differences of measurements of open fields between EPID and diode.

Symmetric open square fields															
Field aperture (cm²)	**6 Mev**			**9 Mev**			**12 Mev**			**15 Mev**			**18 Mev**		
	EPID	**Diode**	**Diff.**	**EPID**	**Diode**	**Diff.**	**EPID**	**Diode**	**Diff.**	**EPID**	**Diode**	**Diff.**	**EPID**	**Diode**	**Diff.**
3.0	1.0152	0.9380	8.23%	1.0087	0.9197	9.67%	1.0055	0.8870	13.36%	1.0018	0.8639	15.97%	1.0006	0.8381	19.39%
4.0	1.0085	0.9680	4.18%	1.0045	0.9702	3.54%	1.0061	0.9475	6.18%	1.0020	0.9365	7.00%	1.0011	0.9260	8.11%
5.0	1.0041	0.9703	3.48%	1.0016	0.9752	2.70%	1.0022	0.9685	3.48%	1.0004	0.9612	4.08%	1.0001	0.9620	3.96%
6.0	1.0043	0.9850	1.96%	1.0025	0.9830	1.99%	1.0038	0.9830	2.12%	1.0015	0.9850	1.68%	0.9998	0.9860	1.40%
8.0	0.9990	1.0074	-0.83%	0.9988	1.0083	-0.94%	1.0001	1.0076	-0.75%	0.9987	1.0022	-0.35%	0.9980	1.0008	-0.28%
10.0	1.0000	1.0000	0.00%	1.0000	1.0000	0.00%	1.0000	1.0000	0.00%	1.0000	1.0000	0.00%	1.0000	1.0000	0.00%
12.0	0.9985	1.0074	-0.89%	0.9993	1.0059	-0.65%	0.9997	1.0040	-0.43%	0.9991	0.9985	0.06%	0.9984	0.9940	0.44%
15.0	0.9996	1.0010	-0.14%	0.9994	0.9993	0.01%	1.0021	0.9949	0.72%	1.0002	0.9908	0.95%	1.0008	0.9864	1.46%
17.0	0.9976	1.0005	-0.29%	0.9990	0.9896	0.95%	0.9998	0.9848	1.52%	1.0005	0.9800	2.09%	1.0011	0.9780	2.36%
20.0	0.9996	0.9950	0.46%	1.0005	0.9851	1.56%	1.0025	0.9805	2.25%	1.0010	0.9830	1.83%	1.0026	0.9780	2.52%

B) Measurements with open rectangular fields

Table 6 summarizes the measurements with EPID and diode for the symmetric rectangular fields of the respective square equivalent field (SEF) referring to stage 2.

Table 6: Output factors and percentage differences of measurements of equivalent square fields between EPID and diode.

Square Equivalent Fields															
SEF (cm²)	6 Mev			9 Mev			12 Mev			15 Mev			18 Mev		
	EPID	Diode	Diff.	EPID	Diode	Diff.	EPID	Diode	Diff.	EPID	Diode	Diff.	EPID	Diode	Diff.
6.0	1.0033	1.0160	-1.25%	0.9987	1.0120	-1.32%	0.9981	1.0050	-0.68%	1.0005	0.9950	0.55%	0.9995	0.9930	0.66%
8.0	0.9991	1.0240	-2.43%	0.9980	1.0250	-2.64%	0.9979	1.0250	-2.64%	0.9991	1.0180	-1.86%	0.9980	1.0170	-1.87%
10.0	0.9988	1.0270	-2.75%	1.0002	0.9990	0.12%	0.9981	0.9920	0.62%	1.0016	0.9820	1.99%	1.0031	0.9770	2.68%
12.0	0.9982	1.029	-3.00%	0.9989	1.0040	-0.51%	0.9963	1.0000	-0.37%	0.9981	0.9940	0.42%	0.9998	0.9820	1.81%
15.0	0.9970	1.0220	-2.45%	0.9990	0.9940	0.50%	0.9981	0.9900	0.82%	1.0001	0.9870	1.33%	0.9995	0.9740	2.61%

Table 7 presents the comparison of readings taken in stage 1 and stage 2 with the diode for open square fields and equivalent open fields, aiming to assess whether the shape of the collimation block cutout influences the output factor measurements and to confirm the validity of equivalent square field values, as the EPID will be used for this purpose in the future.

Table 7: Output factors and percentage differences of measurements of open square fields and square equivalent fields conducted with the diode.

Open square fields vs. Square equivalent fields															
Field aperture (cm²)	6 Mev			9 Mev			12 Mev			15 Mev			18 Mev		
	Open	SEF	Diff.	Open	SEF	Diff.	Open	SEF	Diff.	Open	SEF	Diff.	Open	SEF	Diff.
6.0	0.9850	1.016	-3.05%	0.9830	1.0120	-2.87%	0.9830	1.0050	-2.19%	0.9850	0.9950	-1.01%	0.9860	0.9930	-0.70%
8.0	1.0074	1.0240	-1.62%	1.0083	1.0250	-1.63%	1.0076	1.0250	-1.70%	1.0022	1.0180	-1.55%	1.0008	1.0170	-1.59%
10.0	1.000	1.0270	-2.63%	1.0000	0.9990	0.10%	1.0000	0.9920	0.81%	1.0000	0.9820	1.83%	1.0000	0.9770	2.35%
12.0	1.0074	1.029	-2.10%	1.0059	1.0040	-0.19%	1.0040	1.0000	-0.40%	0.9985	0.9940	0.45%	0.9940	0.9820	1.22%
15.0	1.0010	1.0220	-2.05%	0.9993	0.9940	0.53%	0.9949	0.9900	0.49%	0.9908	0.9870	0.39%	0.9864	0.9740	1.27%

C) Measurements with asymmetric and half-blocked fields

Tables 8 and 9 gather the output factors for the EPID with asymmetrics half-blockeds fields (with the central axis collimated) and the measurements conducted with the four different positions of the block cutouts in the corresponding applicators, compared to the output factor for the open square field, also on the EPID.

Table 8: Output factors for the EPID for asymmetrics half-blockeds fields for 6, 9 and 12 MeV.

Half-Blocked Fields											
			6 MeV			9 MeV			12 MeV		
Block (cm²)	SEF (cm²)	Position	Output	Open Output	Diff.	Output	Open Output	Diff.	Output	Open Output	Diff.
4.0 x 11.0	6.0	Below	1.0067	1.0043	0.24%	1.0010	1.0025	-0.15%	1.0013	1.0038	-0.25%
		Above	1.0047		0.04%	1.0005		-0.20%	1.0011		-0.27%
		Right	1.0057		0.14%	1.0021		-0.04%	0.9998		-0.40%
		Left	1.0046		0.03%	1.0007		-0.18%	0.9994		-0.44%
6.0 x 12.0	8.0	Below	1.0064	0.9990	0.74%	1.0027	0.9988	0.39%	1.0004	1.0001	0.03%
		Above	1.0010		0.20%	0.9982		-0.06%	0.9980		-0.21%
		Right	1.0012		0.22%	0.9994		0.06%	0.9980		-0.21%
		Left	1.0015		0.25%	0.9980		-0.08%	0.9972		-0.29%
7.0 x 18.0	10.0	Below	0.9989	1.0000	-0.11%	0.9989	1.0000	-0.11%	0.9998	1.0000	-0.02%
		Above	0.9998		-0.02%	1.0005		0.05%	0.9984		-0.16%
		Right	0.9985		-0.15%	1.0002		0.02%	0.9981		-0.19%
		Left	0.9982		-0.18%	1.0001		0.01%	0.9996		-0.04%
9.0 x 17.0	12.0	Below	0.9983	0.9985	-0.02%	0.9984	0.9993	-0.09%	0.9976	0.9997	-0.21%
		Above	0.9981		-0.04%	0.9997		0.04%	0.9970		-0.27%
		Right	0.9990		0.05%	0.9970		-0.23%	0.9970		-0.27%
		Left	0.9991		0.06%	0.9993		0.00%	0.9988		-0.09%

In this study, limitations were established for defining the apertures of the collimation blocks to be used. As indicated in the equipment commissioning data, it was observed that the smallest block dimension should not be less than 3.0 cm, particularly for the 6 MeV energy, and the percentage differences increased with increasing energy, as observed in experimental measurements, and as described in the literature [13,18,20]. However, with the comparison of the results found between the EPID and the experimental setup in section A, it was observed that the minimum aperture dimension of the blocks is larger on the EPID, being 5.0 cm², which falls within the acceptable tolerance defined in this study. Some questionable assumptions were made to explain the cause of this phenomenon, such as the possibility of contribution from collimation scattering and

backscatter from the physical layers of the portal detector, defining the first limitation found in the methodology.

Table 9: Output factors for the EPID for asymmetrics half-blockeds fields for 15 and 18 MeV.

Half-Blocked Fields								
			15 MeV			18 MeV		
Block (cm²)	SEF (cm²)	Position	Output	Open Output	Diff.	Output	Open Output	Diff.
4.0 x 11.0	6.0	Below	1.0013	1.0015	-0.02%	1.0020	0.9998	0.22%
		Above	1.0012		-0.03%	1.0006		0.08%
		Right	0.9994		-0.21%	1.0017		0.19%
		Left	1.0008		-0.07%	1.0019		0.21%
6.0 x 12.0	8.0	Below	1.0009	0.9987	0.22%	1.0024	0.9980	0.44%
		Above	0.9992		0.05%	1.0007		0.27%
		Right	0.9993		0.06%	1.0008		0.28%
		Left	0.9981		-0.06%	1.0022		0.42%
7.0 x 18.0	10.0	Below	0,9990	1.0000	-0.10%	1.0016	1.0000	0.16%
		Above	0,9993		-0.07%	1.0011		0.11%
		Right	0,9992		-0.08%	1.0023		0.23%
		Left	0,9983		-0.17%	1.0018		0.18%
9.0 x 17.0	12.0	Below	0,9987	0.9991	-0.04%	1.0023	0.9984	0.39%
		Above	0,9985		-0.06%	0.9999		0.15%
		Right	0,9995		0.04%	1.0009		0.25%
		Left	0,9995		0.04%	1.0028		0.44%

Another influence on the output factor of electron blocks is the superficialization of the Percentage Depth Dose (PDD). This aspect is due to scattering in the collimated block, superficializing the PDD and generating a lower particle fluence than expected at the measurement point for smaller fields. This phenomenon occurs in any electron beam proportionally with increasing energy [13,18,21]. However, the EPID demonstrated a distinct behavior from the water detector, where the output factor measurements for the EPID were overestimated, possibly due to the contribution of collimation scattering and contamination of low-energy photons in electron beams for smaller fields. In this scenario, it is possible to consider adding a copper plate over the portal to investigate if this EPID

behavior changes, as it could modify the reference depth for EPID measurements and become more suitable when measuring at different electron energies.

It was observed that for open symmetric fields measured along the central axis (stage 1) with field apertures ≤ 4.0 cm², the measurements revealed large percentage differences between EPID and diode readings, exceeding the tolerance of up to ±5.0% from the 9.0 MeV energy onwards. This can be explained by the assumptions mentioned earlier, as it fits within the limitation of the methodology for smaller fields. For field apertures of 5.0 cm², the percentage deviations are between ±3.0% and ±5.0%, and from field apertures of 6.0 cm² to 20.0 cm², the results are in accordance with up to ±3.0% percentage deviation [18,19]. Thus, the institution implemented that from 6.0 cm² fields for all energies, the tolerance is ±3.0%, setting the second limitation found for the use of EPID.

For the second stage of the study, it was defined that the recommended minimum aperture of the equivalent square fields is 6.0 cm², as the percentage differences found from this field size fit within the tolerance stipulated in this study as ideal (±3.0%). When comparing the measurements with the diode for open fields and equivalent square fields, it was observed that the percentage differences remained within the ideal limits, except for a single combination of aperture and energy (6.0 cm² and 6 MeV) which showed a variation of -3.05%, still within the acceptable limit of ±5.0%. This indicates that, despite the varied configurations of the collimation blocks, they are compatible, reliable, and meet the tolerances for the output factor at all energies and apertures tested.

In the third stage, the results indicate that EPID measurements can accurately indicate the output factor values off the central axis. For the application of the programming code used, it was necessary to measure the displacement of the central pixel from the collimation block cutout to the central pixel of the open field image, inserting the position coordinates in the x and y directions into the code line to evaluate the central pixel average and obtain the output factor for the half-blocked fields. The first relevant

consideration is the symmetry and flatness of the beams measured in the EPID, which must be periodically evaluated for these measurements to be used, given the dependence of these beam properties.

Image processing was performed using the data saved by the "AM Maintenance" application installed on the 4D console computer, with image acquisition technique in Integrated Image mode, without build-up material, following the recommendation to calibrate the detector at the highest energy available on the equipment (18 MeV) with the largest applicator (25.0 x 25.0 cm^2) to determine the beam fluence, establishing a relationship between the EPID pixel values and the radiation dose. The Dark Field (DF) was measured as the background image and the Flood Field (FF) as the filling image for compensation and gain corrections (variations in the sensitivity of individual photodiodes). The DF measurements were made with the beam turned off to account for the dark current of each pixel, reaching 30.0 frames, and to homogenize the difference in pixel sensitivity, a fill field correction was performed with 200.0 frames (using 200.0 MU). It is also recommended to repeat these detector calibration procedures every time the beam energy changes.

It is worth noting that the images used here, sometimes referred to as "raw" images in the literature, have the DF and FF processing within the AM Maintenance software. However, there are other image processing models in the literature or in software that use EPID images that could affect the data extraction methodology or the development of the code used. Thus, changing the image processing used may affect the methodology developed here and require changes in data extraction.

Regarding the written Python code, an algorithm was developed that established the steps in the following order: identifying the area with the highest pixel count, extracting the in-plane and cross-plane profiles from the central region of the area, and performing statistical analysis of the intersection of these profiles in a 2.0 mm x 2.0 mm area. The same

was done with the reference frames, and the ratio between the desired block apertures and the reference frame was manually performed.

4. CONCLUSIONS

In conclusion, the feasibility of obtaining the output factor through measurements performed on the EPID was demonstrated by comparing them with measurements using a water phantom and a diode detector. This method proved to be suitable for square, rectangular, and asymmetric fields, including half-blocked fields (with the central axis collimated). The methodology was found to be quick to execute and required minimal instrumentation, making it useful for the routine of a Radiotherapy Service.

It is important to note, however, that the technique has limitations regarding field apertures for each energy, and the definition of tolerances to be used depends on institutional validation. Additionally, the developed codes for this study could further evolve to become more simplified and automated, although they are already viable for the routine tasks of a medical physicist.

CONFLICT OF INTEREST

All authors declare that they have no conflicts of interest.

REFERENCES

[1] INSTITUTO NACIONAL DE CÂNCER JOSÉ ALENCAR GOMES DA SILVA. **Estimativa 2023: Incidência de câncer no Brasil.** Rio de Janeiro: INCA, 2022. ISBN 978-65-88517-10-9.

[2] INSTITUTO NACIONAL DE CÂNCER JOSÉ ALENCAR GOMES DA SILVA. **Curso a distância – O Elétron na Radioterapia.** Rio de Janeiro: INCA, 2013. IBSN 85-7318-1o1-X.

[3] NEBBIA, J. F.; ORTHOLAN, C.; GERARD, J. P. Radiotherapy in cancer pain management. European Journal of Cancer Supplements, v. 3, n. 3, p. 87-96, 2005.

[4] SONG, CHANGHOON et al. **Adjuvant single-fraction radiotherapy is safe and effective for intractable keloids.** Journal of radiation research, v. 55, n. 5, p. 912-916, 2014.

[5] MENEZES Neto, B. F. D. (2022). **Construção do protocolo de tratamento de queloide do Hospital das Clínicas da Faculdade de Medicina de Botucatu.** 2022. Dissertação (Mestrado em Medicina) - Universidade Estadual Paulista "Júlio de Mesquita Filho" – Faculdade de Medicina, Botucatu, 2022.

[6] OLIVEIRA JÚNIOR, B. et al. **Comparative study between the radiotherapy treatment with electrons and beta-therapy after keloid surgery.** Surgical & Cosmetic Dermatology, v. 1, n. 2, p. 53-57, 2007.

[7] CARVAJAL, Claudia C. et al. **Postoperative radiotherapy in the management of keloids.** ecancer medical science, v. 10, 2016.

[8] OLIVEIRA JÚNIOR, B. et al. **Keloid treatment using post operative radiotherapy with electron beams: a comparative randomized study of two methods.** Surg Cosmet Dermatol, v. 5, n. 1, p. 16-26, 2013.

[9] JUNIOR, Otsuka; FUMIYUKI, Lauro. **E-book sobre cicatrizes patológicas para o não especialista.** 2019.

[10] GOMES Olga Santana et al. **Cirurgia plástica no Brasil: uma análise epidemiológica.** Revista Eletrônica Acervo Científico, v. 24, p. e7375-e7375, 2021.

[11] MINISTÉRIO DA SAÚDE. Biblioteca Virtual em Saúde. Ministério da Saúde; [21/06/2021]. Available at: https://bvsms.saude.gov.br/queloide/. Acsessed on: 5 jul. 2023.

[12] KHAN, Faiz M. (Ed.). **The physics of radiation therapy.** Lippincott Williams & Wilkins, 2010. ISBN 978-1-4511-8245-3.

[13] BULUT, Ahmet. **Predicting electron insert output factors at nominal and extended source to surface distance.** Louisiana State University and Agricultural & Mechanical College, 2002.

[14] SILVEIRA, Thiago Bernardino da. **Implementação de EPID para avaliação e controle de qualidade de feixes clínicos em radioterapia.** Tese de Mestrado. Instituto de Radioproteção e Dosimetria da Comissão Nacional de Energia Nuclear.

[15] DING, Aiping; XING, Lei; HAN, Bin. **Development of an accurate EPID based output measurement and dosimetric verification tool for electron beam therapy.** Medical Physics, v. 42, n. 7, p. 4190-4198, 2015.

[16] WANG, Y. et al. Quality assurance of electron beams using a Varian electronic portal imaging device. Physicsin Medicine & Biology, v. 58, n. 16, p. 5461, 2013.

[17] RIBEIRO, Rosane Moreira. **Implementação de Teste para Controle de Qualidade de Feixe de Elétrons utilizando o EPID da Varian.** Trabalho de Conclusão de Residência. Instituto Nacional de Câncer José Alencar Gomes da Silva.

[18] GIBBONS, John P. et al. **Monitor unit calculations for external photon and electron beams: Report of the AAPM Therapy Physics Committee Task Group No. 71.** Medical physics, v. 41, n. 3, p. 031501, 2014.

[19] STERN, Robin L. et al. **Verification of monitor unit calculations for non IMRT clinical radiotherapy: report of AAPM Task Group 114.** Medical physics, v. 38, n. 1, p. 504-530, 2011.

[20] MCPARLAND, Brian J. **Methods of calculating the output factors of rectangular electron fields.** Medical Dosimetry, v. 14, n. 1, p. 17-21, 1989.

[21] CHOI, David R.; MOBIT, Paul N.; BREITMAN, Karen E. **The clinical implementation of a method for calculating the output factor and percent depth dose for an electron beam.** Physics in Medicine & Biology, v. 48, n. 7, p. 899, 2003.

LICENSE